Charging and Transport Dynamics of a Flow-Through Electrode Capacitive Deionization System

Supporting information

Yatian Qu,[a,b] Patrick G. Campbell,[b] Ali Hemmatifar,[a] Jennifer M. Knipe,[b] Colin K. Loeb,[b] John J. Reidy,[c] Mckenzie A. Hubert,[d] Michael Stadermann[b] and Juan G. Santiago[a]**

[a] Department of Mechanical Engineering, Stanford University Stanford, CA 94305, USA

[b] Lawrence Livermore National Laboratory, 7000 East Avenue, Livermore, CA, USA.

[c] Department of Chemistry, Stanford University Stanford, CA 94305, USA

[d] Department of Chemical Engineering, Stanford University Stanford, CA 94305, USA

*To whom correspondence should be addressed. E-mails: juan.santiago@stanford.edu and stadermann2@llnl.gov

This document contains supplementary information and figures further describing our formulation of volume-averaged model and area-averaged model; fitting parameter extraction process with experimental data; and additional simulation results from the area-averaged model.

- S-1: Derivation of one-dimensional transport equation in macropores
- S-2: Expressions of salt adsorption and electrode surface charge density in Gouy-Chapman-Stern electrical double layer model
- S-3: Detailed derivation of zero-dimensional ODE for volume-averaged model
- S-4: Analytical solutions to ODEs of volume-averaged model
- S-5: Area-averaged model of flow-through electrode CDI system with constant voltage operation
- S-6: Fitting parameter extraction from near-equilibrium experiments
- S-7: Plot of cell potential over time during charging
- S-8: Spatiotemporal plots of salt concentrations predicted by the area-averaged model

S-1: Derivation of one-dimensional transport equation in macropores

We here present the derivation of one-dimensional transport equation in macropores (Equation 2 in the main paper). We start with the general form of MPE transport equation,

$$p_M \frac{\partial}{\partial t}(c_i) + \nabla \cdot \boldsymbol{N}_i = a j_{in}. \tag{1}$$

Here, c_i is the concentration of ion species i in the pores. p_M is the porosity associated with macropores (the volume fraction of the pores contributing to mass transport pathways). $\boldsymbol{N}_i$ is the cross-sectional area-averaged (solid and liquid phase) ion flux, including contributions from advection, dispersion, and electromigration. j_{in} is the molar flux averaged over the interfacial area between the electrode matrix and liquid phase. a is the specific interfacial area, defined as the surface area of the porous electrode per unit volume of the total electrode.

In one-dimensional and binary electrolyte system, we can write transport equation for cations and anions as:

$$p_M \frac{\partial c_+}{\partial t} + u_{sup} \frac{\partial c_+}{\partial x} - \frac{p_M \mu_+}{\tau V_T} \frac{\partial \phi}{\partial x} - p_M D_{BF,+} \frac{\partial^2 c_+}{\partial x^2} = a j_+ \tag{S2}$$

$$p_M \frac{\partial c_-}{\partial t} + u_{sup} \frac{\partial c_-}{\partial x} + \frac{p_M \mu_-}{\tau V_T} \frac{\partial \phi}{\partial x} - p_M D_{BF,-} \frac{\partial^2 c_-}{\partial x^2} = a j_- \tag{S3}$$

Here u_{sup} is the superficial velocity. μ_+ and μ_- are electrophoretic mobilities for cation and anions respectively. $D_{BF,+}$ and $D_{BF,-}$ are the one-dimensional Burnett-Frind hydrodynamic dispersion coefficients which approximate the effects of longitudinal dispersion of ion species due to both mechanical spreading and molecular diffusion in porous media. We assume that $D_+ = D_- = D$ and $D_{BF,+} = D_{BF,-} = D_{BF}$. V_T is thermal voltage ($V_T = kT/e$, k and T being Boltzmann constant and temperature). τ is tortuosity of electrode material.

In macropores, we have $c_+ = c_- = c$. Adding Eq. S2 and S3, we cancel the eletromigration flux term and arrive at the following equation:

$$p_M \frac{\partial c}{\partial t} + u_{sup} \frac{\partial c}{\partial x} - p_M D_{BF} \frac{\partial^2 c}{\partial x^2} = \frac{a}{2}(j_+ + j_-) \tag{S4}$$

The right-hand side of Equation S4 represents the molar ion flux through the interfacial area between electrode matrix and liquid phase. We can relate this ion flux to the local salt adsorption rate $-p_m \frac{\partial(a\Gamma)}{\partial t}$. Equations S4 then yields to the mass transport equation,

$$p_M \frac{\partial c}{\partial t} + u_{sup} \frac{\partial c}{\partial x} - p_M D_{BF} \frac{\partial^2 c}{\partial x^2} = - p_m \frac{\partial(a\Gamma)}{\partial t}. \quad \text{(S5)}$$

which is Equation 2 in the main paper.

S-2: Expressions of salt adsorption and electrode surface charge density in Gouy-Chapman-Stern electrical double layer model

In the Gouy-Chapman-Stern model, the expressions for the local charge density on the electrode surface (in unit of moles per area) σ is:

$$\sigma = 4 \frac{c_\infty}{\kappa} \sinh(\frac{1}{2} \Delta\phi_{diff}) \quad \text{(S6)}$$

where c_∞ is the ion concentration in the bulk solution. κ is the inverse of the Debye length. $\Delta\phi_{diff}$ is the potential drop across electrical double layer.[1]

The expression for salt adsorption Γ in units of moles per electrode surface area is:

$$\Gamma = 8 \frac{c_\infty}{\kappa} \sinh^2(\frac{1}{4} \Delta\phi_{diff}) \,. \quad \text{(S7)}$$

[1]

S-3: Detailed derivation of zero-dimensional ODE for volume-averaged model

We here present detailed derivation of unsteady volume-averaged model. We start with the one-dimensional transport governing equation (Equation 3) in the main paper.

$$p_M \frac{\partial c}{\partial t} + u_{sup} \frac{\partial c}{\partial x} - p_M D_{BF} \frac{\partial^2 c}{\partial x^2} = -p_m \lambda \frac{\partial(a\sigma)}{\partial t}. \quad \text{(S8)}$$

As we defined in the main paper, the one-dimensional Burnett-Frind hydrodynamic dispersion coefficient D_{BF} relates to longitudinal dispersivity parameter α_L and molecular diffusivity as $D_{BF} = \alpha_L u_{sup} + D_{eff}$. Here D_{eff} is the effective molecular diffusivity. This diffusivity can be interpreted as the molecular diffusivity D corrected to account for tortuosity (and is here equal to the molecular diffusivity D divided by tortuosity).

We perform volume integration over the entire cell V_0 on both sides:

$$\int_{V_0} p_M \frac{\partial c}{\partial t} dV + \int_{V_0} u_{sup} \frac{\partial c}{\partial x} dV - \int_{V_0} p_M D_{BF} \frac{\partial^2 c}{\partial x^2} dV = \int_{V_0} - p_m \lambda \frac{\partial (a\sigma)}{\partial t} dV. \quad \text{(S9)}$$

We define a cell average concentration as

$$p_M V_0 \frac{\partial \bar{c}}{\partial t} \approx \int_{V_0} p_M \frac{\partial c}{\partial t} dV \quad \text{(S10)}$$

We now substitute the expression for cell average concentration to Equation S9 and apply divergence theorem. The volume-integrated transport equation then becomes:

$$p_M V_0 \frac{\partial \bar{c}}{\partial t} + (u_{sup} A_m c - p_M D_{BF} \frac{\partial c}{\partial x} A_m)\Big|_{out} - (u_{sup} A_m c - p_M D_{BF} \frac{\partial c}{\partial x} A_m)\Big|_{in} = -\frac{\lambda I_0}{F} \quad \text{(S11)}$$

To further simplify the equation, we approximate $\bar{c} \approx \frac{1}{2}(c_0 + c_e)$ and $\frac{\partial c}{\partial x}\Big|_{in} = \frac{c_e - c_0}{L_s + 2L_e}$ at cell inlet and approximate $\frac{\partial c}{\partial x}\Big|_{out} = \frac{c_e - c_0}{L_s + 2L_e}$ at the outlet of the domain as boundary conditions.

Equation S11 then becomes:

$$\frac{\partial c_e}{\partial t} + \frac{2Q}{p_M V_0}(c_e - c_0) = -\frac{2\lambda I_0}{p_M V_0 F} \quad \text{(S12)}$$

We now arrive at Equation 11 presented in the main paper.

S-4: Analytical solutions to ODEs of volume-averaged model

We analytically solve the ODEs of volume-averaged model (Equation 12 in the main paper).

$$\begin{cases} \frac{\partial c_e}{\partial t} + \frac{2Q}{p_M V_0}(c_e - c_0) = -\frac{I_0^2}{4 p_M p_m V_0 V_e c_0 F^2} t & (\lambda < 1) \\ \frac{\partial c_e}{\partial t} + \frac{2Q}{p_M V_0}(c_e - c_0) = -\frac{2 I_0}{p_M V_0 F} & (\lambda = 1) \end{cases} \quad \text{(S13)}$$

Equation S13 is the general formulation of unsteady volume-averaged model and it applies to both advection-limited and dispersion limited regime. For the ODE in the regime of $\lambda < 1$, we group known parameters as:

$$\begin{cases} A = \dfrac{2Q}{p_M V_0} \\ \mathrm{B} = -\dfrac{I_0^2}{4p_m p_M V_0 V_e c_0 F^2} \end{cases} \tag{S14}$$

The initial condition for this ODE is $c_e = c_0$ at $t = 0$. We then derive the solution using the integral factor method as:

$$c_e(t) = c_0 - \left(\frac{B}{A^2}\right)(1 - e^{-At}) + \left(\frac{B}{A}\right)t\,, \quad \left(t < \frac{8p_M V_e c_0 F}{I_0}\right) \tag{S15}$$

We note that this solution is only valid for $\lambda < 1$. Therefore, Equation S15 is the solution to c_e at the early charging phase, from $t = 0$ to $t_\lambda = \frac{8p_M V_e c_0 F}{I_0}$.

In a similar manner, for ODE in the regime of $\lambda = 1$, we group the known parameters as:

$$\begin{cases} A = \dfrac{2Q}{p_M V_0} \\ \mathrm{C} = -\dfrac{2I_0}{p_M V_0 F} \end{cases} \tag{S16}$$

The initial condition is $c_e(t = t_\lambda)$ from Equation S15 at $t = t_\lambda$. The solution (using integral factor method) is then:

$$c_e(t) = \left(\frac{C}{A}\right) + k_1(e^{-At}) + c_0\,, \qquad \left(t \geq \frac{8p_M V_e c_0 F}{I_0}\right) \tag{S17}$$

where the parameter k_1 is determined by the initial condition. Equations S15 and S17 are summarized in the text of the main paper. In advection-limited regime, the predictions of effluent concentrations by volume-averaged model are shown in Figure 2 in the main paper.

S-5: Area-averaged model of flow-through electrode CDI system with constant voltage (CV) operation

As mentioned in the main text, the higher fidelity area-averaged model with modified Donnan approach and native charge can be modified to constant voltage (CV) operation. We here present the full set of equations for CV operations.

Governing equations for mass transport and salt charge balance in macropores are respectively:

$$p_M \frac{\partial c}{\partial t} + u_{sup} \frac{\partial c}{\partial x} - p_M D_{BF} \frac{\partial^2 c}{\partial x^2} = -p_m \frac{\partial w}{\partial t} \tag{S21}$$

$$\frac{p_M}{\tau} \mu \frac{\partial}{\partial x}\left(c \frac{\partial \phi}{\partial x}\right) = p_m \frac{\partial q}{\partial t} \tag{S22}$$

Equation for charge balance and in the electrode and electrolyte matrix is:

$$2q + q_{native} + q_e = 0 \,. \tag{S23}$$

To relate electrical charge q_e to the micropore potential drop $\Delta\phi_m$:

$$\Delta\phi_m = q_e \frac{F}{C_m} \tag{S24}$$

Potentials relation in the system:

$$\Delta\phi_m + \Delta\phi_D + \phi = \phi_{ext} \tag{S25}$$

Equation S21 – S25 and boundary and initial conditions (see Figure 1b in the main paper) complete the formulation of area-averaged models for fteCDI cell with CV operations. The definitions of variables and parameters are the same as those in the main paper. We note that in CV simulations, the potential of electrode phase ϕ_e becomes a known value as ϕ_{ext}. As a result, the full set of equations for CV conditions has one equation fewer than that of CC conditions (Equation 15 – 20 in the main paper).

Figure S1(a) shows the effluent concentration of a fteCDI cell operating at 1.2V constant voltage with constant flow at a flow rate of 0.48 mL/min. The parameters used in CV simulations have the same values as those used in CC simulations in the main text. In CV operations, effluent concentration demonstrates different features than those of CC

charging. The effluent concentration quickly reaches a minima and then gradually returns to feed concentration level. The fast desalination at beginning was caused by high electrical current flux in the electrode matrix. As salt adsorption saturates, the salt concentration gradually increases.[2] Figure S1(b) is the spatiotemporal plot of salt concentrations in a fteCDI cell (time and position along the 1D cell model in the ordinance and abscissa, respectively). This plot demonstrates the dynamic change of salt concentrations over time inside a fteCDI.

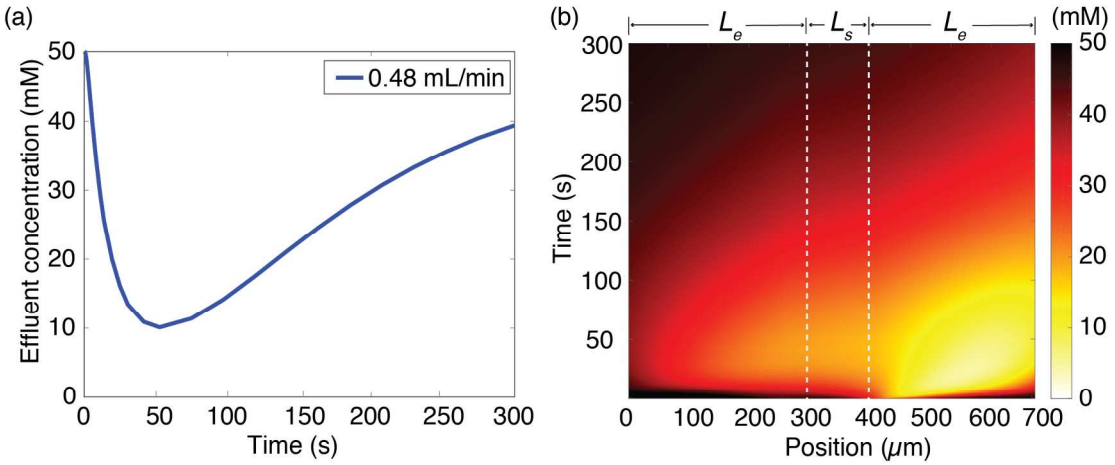

Figure S1. (a) Simulated effluent concentration versus time and (b) spatiotemporal representation of in situ deionization dynamics of a fteCDI cell operated with CV charging at 1.2 V and with constant flow rate at 0.48 mL/min. These simulations are performed with the high fidelity area-averaged model with CV conditions.

S-6：Fitting parameter extraction from near-equilibrium experiments

We used measured values of equilibrium adsorbed salt and transferred charge at constant voltage charging to estimate the model parameters. To this end, we applied external voltages of 0.4, 0.6, 0.8, and 1 V across the cell at fixed 0.48 mL/min flow rate for 0.5 h and discharged the cell at 0 V for 0.5 h. We calculate the adsorbed salt Γ and transferred charge Σ (both in units of moles per electrodes mass) as follows.[3]

$$\Gamma = \frac{1}{m_{tot}} \int Q(c_0 - c_e) dt \tag{S23}$$

$$\Sigma = \frac{1}{m_{tot}} \int (I_{ext} - I_{leak}) dt \tag{S24}$$

where m_{tot} is total (dry) mass of electrodes, Q is flow rate, c_e is area-averaged effluent salt concentration, I_{ext} is cell electric current, and I_{leak} is the leakage current (measured current at the end of charging phase, likely due to Faradaic reactions at the electrode surface).

We note that equilibrium data are governed only by double layer model, external voltage (or current), and influent concentration. Cell geometry, flow rate, and dispersion phenomena do not affect the equilibrium solutions. This means that equilibrium data is independent of α_L. Thus, we will use effluent concentration data as well.

We first solved the set of equations S21-S25 for a variety of C_m, p_m, and q_{native} values at steady state (infinite time) as a function of external voltage. We then minimized the sum of mean square error of adsorbed salt Γ and transferred charge Σ. All numerical simulations were performed with a commercially available finite element simulation software (COMSOL Multiphysics, 5.1, Burlington, USA)

Figure S2 shows the measured values (from experiments) and the best fit line in units of milimoles. The estimated values are C_m = 120 F/cm^3, p_m= 0.1, and q_{native} = 100 moles/m^3. We subsequently used dynamic measurements of effluent salt concentration to determine α_L at fixed C_m, p_m, and q_{native}. To this end, we varied α_L such that the temporal effluent salt concentration from the model matches that of experiments. Our final estimate is α_L=10^{-4} m.

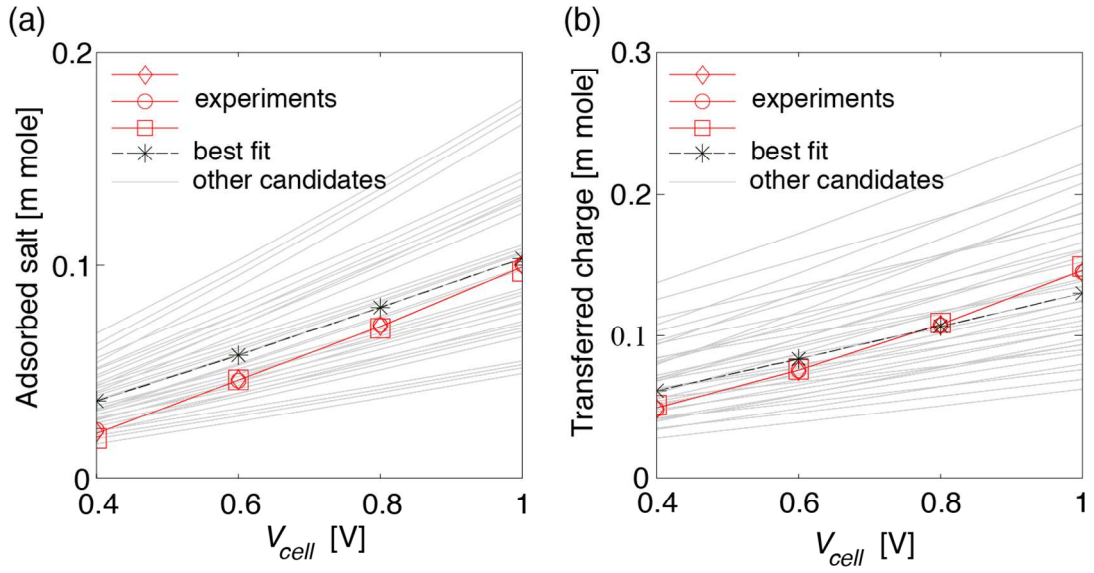

Figure S2. Experimentally measured and numerically simulated adsorbed salt and transferred charge. Gray lines are numerical simulation results with different sets of parameters. The red lines with diamond, round and square symbols are experimental data. The black line with star symbol is the best-fit simulation result.

S-7: Plot of cell potential over time during charging

Figure S3 shows the cell potential over time during 50 mA constant current charging with flow rates at 2.5, 5.1, 7.7, 10.3 and 12.8 mL/min. The black dashed line serves as a visual guide to indicate the linear charging behavior of an ideal capacitor. As we mentioned in our main text (line 487), parasitic reactions during CDI charging provide current leakage paths, and therefore lower the rate of charge accumulation in cell. The voltage profiles below show that cell potential deviates from ideal capacitor charging around 150 s when the cell voltage reaches 0.7 V. We attribute this deviation to the charge loss associated with parasitic reactions such as the reduction of dissolved oxygen.

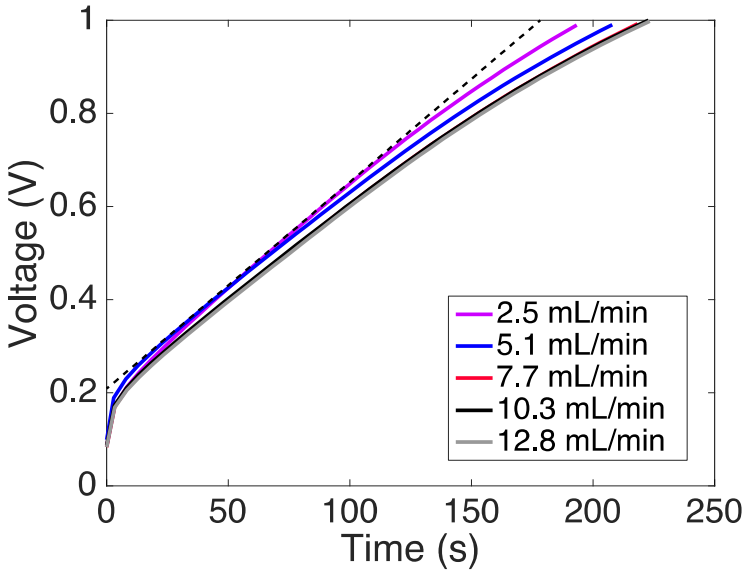

Figure S3. Plot of cell potential over time during charging at 50 mA and with flow rates of 2.5, 5.1, 7.7, 10.3 and 12.8 mL/min. The black dashed line serves as a visual guide to indicate the linear charging behavior of an ideal capacitor. Voltage profiles start to deviate from ideal capacitor charging because of charge loss around 0.7 V and 150 s. We hypothesize that the charge loss is caused by parasitic reactions, such as the reduction of dissolved oxygen.

S-8: Spatiotemporal plots of salt concentrations predicted by the area-averaged model

We present the spatiotemporal plots of salt concentrations inside a fteCDI cell predicted by the area-averaged model at flow rates of 0.22 mL/min, 2.5 mL/min and 12.8 mL/min. The Peclet-type numbers Pe^* are 1.3, 8.8 and 11 respectively. The cell is charged with constant current at 50 mA. The ordinance in the plots is charging time and the abscissa is the position along the 1D cell. As mentioned in the main paper, the flow rate of 0.22 mL/min is in dispersion-limited regime, and the flow rates of 2.5 and 12.8 mL/min are in the advection-limited regime. As shown in Figure S4, our model captures the non-uniform charging of the electrodes and demonstrates the in situ salt removal dynamics inside a fteCDI cell. In the main paper, Figure 3(a) shows that the volume-averaged model predicts the leveling off of effluent concentrations at a time scale faster than the area-averaged model. We attribute this difference to the effect of non-uniform charging of the electrode, which is only captured by the area-averaged model.

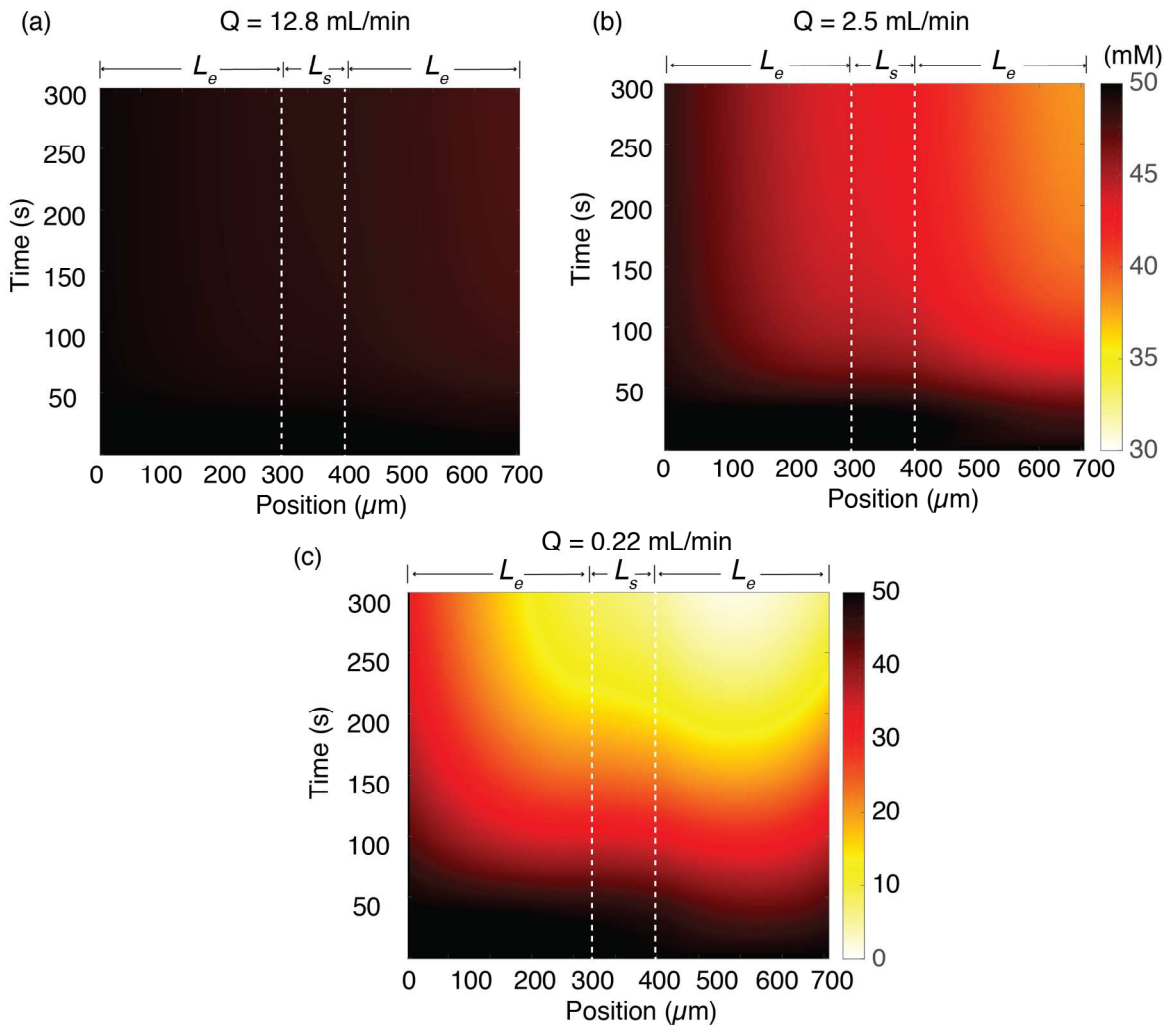

Figure S4. Spatiotemporal plots of simulated salt concentration in a fteCDI cell, with constant current charging at 50 mA and flow rates of (a) 0.22 mL/min (Pe^*=1.3), (b) 2.5 mL/min (Pe^* = 8.1) and (c) 12.8 mL/min (Pe^*=11). These simulation results demonstrate the salt removal dynamics and inhomogeneous charging inside a fteCDI cell.

References

1. Biesheuvel, P. M.; Limpt, B. v.; Wal, A. v. d., Dynamic Adsorption/Desorption Process Model for Capacitive Deionization. *The Journal of Physical Chemistry C* **2009**, *113*, 5636 - 5640.
2. Qu, Y.; Campbell, P. G.; Gu, L.; Knipe, J. M.; Dzenitis, E.; Santiago, J. G.; Stadermann, M., Energy Consumption Analysis of Constant Voltage and Constant Current Operations in Capacitive Deionization. *Desalination* **2016**, *400*, 18-24.
3. Hemmatifar, A.; Stadermann, M.; Santiago, J. G., Two-Dimensional Porous Electrode Model for Capacitive
Deionization. **2015**.